Design and Analysis of Single-Phase Grid-Tied Inverter With PDM MPPT-Controlled Converter

Akif Karafil, Harun Ozbay, and Selim Oncu

***Abstract*—In this article, a novel method is presented for maximum power point tracker (MPPT) system to increase efficiency. For this purpose, maximum power obtained from photovoltaic (PV) panels by pulse density modulation (PDM)-controlled high-frequency series-resonant converter was transferred to grid by a single-phase inverter. The resonant converter and the single-phase inverter circuits used in the system were analyzed, designed, simulated, and implemented. The designed series-resonant converter was operated at resonant frequency for different solar radiation conditions using the PDM control technique, and therefore the maximum power point was tracked. Soft switching was achieved by continuously tracking the resonant frequency. Simulated and experimental results were presented for 600 W prototype by operating the MPPT converter over 100 kHz. The MPPT efficiency was obtained as 99% and above. The maximum power tracking of the PV panels was achieved using the perturb and observe (P&O) algorithm with PDM technique. The generated PV power was transferred to the single-phase grid by an LCL-filtered inverter. Proportional integral controller was preferred in the control of single-phase grid-tied inverter.**

***Index Terms*—DC-AC power converters, energy efficiency, maximum power point trackers, power control, resonant inverters.**

I. Introduction

ENERGY sector has a significant share in the economic growth of countries. Although fossil fuels have been used to generate most of the required energy, increasing costs and the environmental problems caused by them are undeniable. Therefore, it is very important to increase the use of renewable energy sources which are economical, inexhaustible, and clean [1]. Solar energy systems, which are among the renewable energy sources, are clean, easy to use and to install. Electricity is obtained from the solar energy using PV systems. PV systems consist of PV panels and converter (dc–dc, dc–ac) circuits. Sun light is directly converted into electrical energy by semiconductor materials used in PV panels. Generated electrical energy is transferred to batteries, load, or grid by converter circuits depending on the operation condition [2]–[4].

Output power of PV panels changes continuously depending on changing environmental conditions such as temperature, shading, and solar radiation level. In this case, the power obtained from PV panels also varies. Therefore, a more efficient and accurate MPPT algorithm should be designed in order to improve the operating efficiency of PV generation systems [5], [6]. In the literature, a large number of MPPT methods have been proposed to track the maximum power point (MPP) for PV panels under various environmental conditions. Among these methods, perturb and observe (P&O) method is widely used in PV systems because of its high efficiency, simplicity, and ease of implementation [7], [8].

The size of dc–dc converter in the PV system is desired to be small, light, and highly efficient, and switching losses must be low in order to operate with high efficiency. However, during switching, hard switching condition occurs since either the current passing through the power switch or the voltage on the switch terminals is not zero. High switching losses caused by hard switching limit the frequency of the converter, resulting in low efficiency and damage to switches. Lossless soft switching can be achieved by adding an inductor (L) and a capacitor (C) to the conventional converter circuit. Resonant converters and soft switching techniques have been used to reduce the switching losses at high operating frequencies. Therefore, smaller passive elements and heat sinks are used in the design, which reduces the size and the cost of the circuit [9]–[12].

Many control techniques such as frequency control, pulsewidth modulation (PWM), phase shift, and bus voltage control are used for the power control of the converter circuit. However, for these control techniques, soft switching cannot be guaranteed for all power values [13]. Since the power produced by the panels in PV systems is not constant all the time, it is not possible to track the MPP by operating with resonant converter at constant operating frequency. PDM control is used for power tracking by providing soft switching conditions at each power point in resonant converter circuits. The required output power is achieved gradually by PDM control by deleting some control pulses of the converter operating at resonant frequency. Moreover, in this control technique, frequency can be kept constant and a wide range of power control can be provided [14], [15].

With the resonant converter used in the system, the maximum power obtained from PV panels is transferred to the grid by the grid-tied inverter. For grid-tied inverters, total harmonic distortion (THD) value of the fundamental frequency current

Manuscript received May 30, 2019; revised August 16, 2019; accepted September 22, 2019. Date of publication September 29, 2019; date of current version February 11, 2020. This work was supported in part by the Karabuk University Research Projects Fund under Grant KBU-BAP-15/2-DR-005. Recommended for publication by Associate Editor A. Safaee. *(Corresponding author: Akif Karafil.)*

A. Karafil is with Bilecik Şeyh Edebali Üniversitesi, 11230 Bilecik, Turkey (e-mail: akif.karafil@bilecik.edu.tr).

H. Ozbay is with Bandirma Onyedi Eylul Universitesi, 10200 Bandirma, Turkey (e-mail: hozbay@bandirma.edu.tr).

S. Oncu is with Karabuk University, 78050 Karabuk, Turkey (e-mail: soncu@karabuk.edu.tr).

Color versions of one or more of the figures in this article are available online at http://ieeexplore.ieee.org.

Digital Object Identifier 10.1109/TPEL.2019.2944617

transferred to the grid must be below 5% according to international IEC 61727 and IEEE 1547 standards [16]. In order to transfer the current to the grid in accordance with these standards, a filter must be used at the output of the inverter or the design must be made accordingly. The most commonly used filter type is LCL filter with its smaller size and lower costs [17], [18]. In grid-tied inverters, the control system can control the parameters such as voltage, current, and power. Proportional integral (PI) and proportional resonant (PR) controllers are generally preferred for current control of inverters which are used with PV systems without affecting the dynamics of the control unit [19], [20].

When literature is examined, Fujita and Akagi [13] provided induction heater power control by phase-locked loop (PLL)-based 16 PDM technique of full-bridge series resonant inverter for 4 kW, 450 kHz frequency. A similar study was conducted by Esteve *et al.* [15] for induction heating applications for 50 kW power and 150 kHz frequency. Li *et al.* [20] used PDM technique for 50 W wireless power transfer to achieve maximum efficiency. Borekci [21] performed the control of dimmer circuit used in the lighting system by PDM technique. Korošec *et al.* [22] designed a PDM microinverter operating at 100 W and performed experimental studies. Fan *et al.* [23] used the PDM technique to conduct inductive power transfer in rail vehicles. Jiang *et al.* [24] cascaded boost converter with bidirectional half-bridge. MPPT algorithm was used as variable step size in the system. The full-bridge single-phase PWM inverter was synchronized with LCL filter and transferred to the grid.

Even though many studies are conducted using the PDM control technique, PDM-controlled MPPT has not been used for grid-tied PV generation system. On the other hand, the PDM control technique has a significant value in MPPT system with resonant converter since it increases the limited operating frequency and overcomes switching losses, which are the basic problems of conventional hard-switched MPPTs. Therefore, PDM-controlled MPPT system can operate at higher efficiency and can be more effective. In light of this information, in this article, a new control method is presented to improve the efficiency of MPPT systems. For this purpose, MPPT system with high-frequency series-resonant converter, which is used to transfer electrical energy obtained from PV panels to single-phase grid, was designed by using the PDM control technique; simulation and experimental studies were performed. The study was performed by cascading two converters. The first converter includes a full-bridge series-resonant converter. The control of series-resonant converter which can be operated at different solar radiation conditions for PV panels was carried out by PLL-based 16 PDM MPPT control. With PLL technique, zero transitions of the current signal on series-resonant side were detected so that the converter could operate in zero current switching (ZCS) conditions. P&O MPPT with 16 PDM provided power control by deleting some of the control pulses according to the power of PV panels without any change in switching frequency and the turn ON duration of the switch. The second part is a grid-tied inverter. The analyses of PI current controller LCL-filtered single-phase grid-tied inverter were conducted and the simulation and experimental studies were carried out. Full-bridge series-resonant converter and single-phase grid-tied inverter parts were cascaded and the simulation and experimental studies for the whole system were carried out. A TMS320F28335 DSP was used to control both converters in the system.

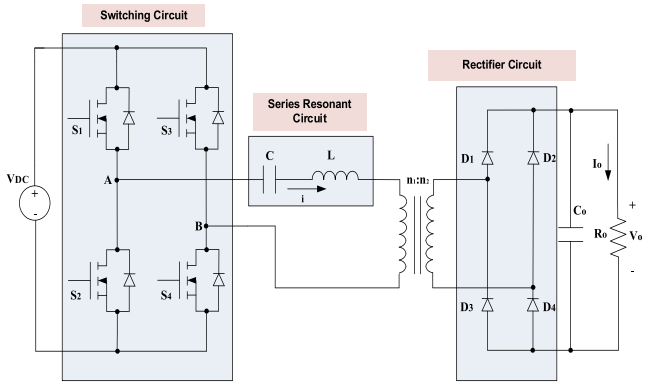

Fig. 1. Series resonant converter circuit.

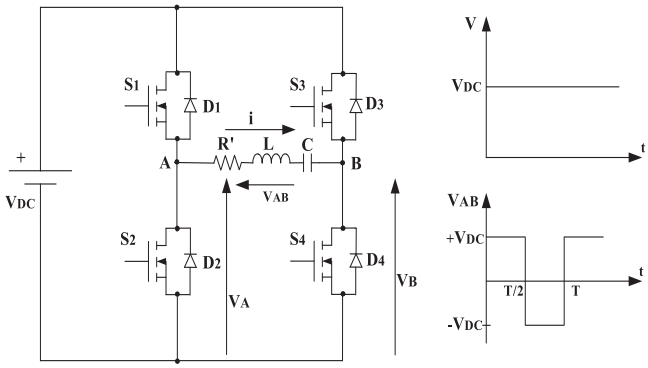

Fig. 2. Full-bridge series-resonant inverter circuit scheme.

II. Analysis and Control of PDM-Controlled Full-Bridge Series-Resonant Converter

A. Series-Resonant Converter

Fig. 1 presents the series-resonant converter circuit. The resonant circuit in the series-resonant converter is obtained by series connection of a resonant capacitor and a resonant inductor.

When the switching frequency (f_s) of the series-resonant converter is equal to the resonant frequency (f_r), impedance of the circuit is at minimum $(f_s = f_r)$. Inverter output voltage and current are on phase. As a result, ZCS is achieved at both turn ON and turn OFF transients [25], [26].

The equivalent series-resonant inverter circuit scheme of the converter is given in Fig. 2.

In the analysis of the circuit, converting the load resistance to the ac-equivalent resistance value should be taken into account. The ac-equivalent resistance value is obtained by the following equation [27]:

$$R' = \frac{8.\left(\frac{n_1}{n_2}\right)^2}{\pi^2}.R_o \tag{1}$$

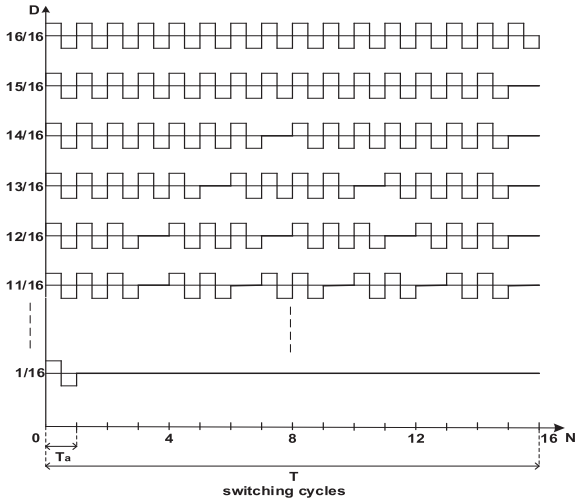

Fig. 3. 16 PDM patterns.

where R' is the ac-equivalent resistance, R_o is the load resistance, and n_1:n_2 is the turns ratio of the transformer. Resonant frequency (f_r), damping coefficient (α), and the quality factor (Q), which are the basic equations of the circuit, are given below, respectively [28], [29]

$$f_r = \frac{1}{2\pi\sqrt{LC}} \tag{2}$$

$$\alpha = \frac{R'}{2L} \tag{3}$$

$$Q = \frac{\omega_r L}{R'}. \tag{4}$$

B. PDM Control Technique

The power that PV panels can produce is not constant all the time. Therefore, it is not possible to achieve soft switching for both turn ON and OFF transients at a fixed frequency with PWM, phase shift, or frequency modulation. PDM control technique enables the resonant converter to control the power at constant operating frequency by maintaining soft switching conditions at each power point of the PV system.

PDM control technique is a set of commands. Power control is performed by deleting some of the control pulses according to the command sequences without any changes in the switching frequency and the turn ON duration of the switch. The output power of the converter decreases as the number of the deleted control pulses increases [13]–[15]. Fig. 3 shows the PDM switching patterns.

The rows show 16 resonant cycles formed to control the inverter switches. The time of each cycle is equal to the resonant period time ($T = NT_a$). When the maximum PDM length $N = 16$ is selected, pulse density D varies from 1/16 to 16/16. In the case of 1/16, the lowest power is achieved and the maximum power is provided in 16/16 [14], [30].

The inverter operates in three switching modes to adjust the output power. These switching modes are given in Fig. 4.

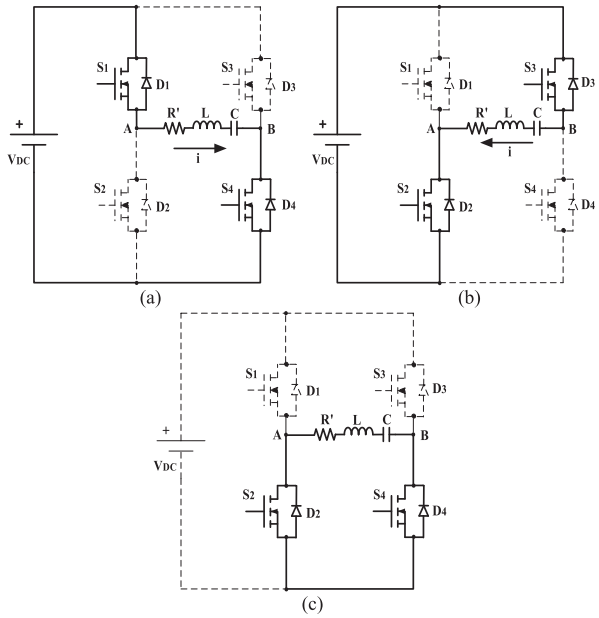

Fig. 4. Switching modes. (a) Mode I. (b) Mode II. (c) Mode III.

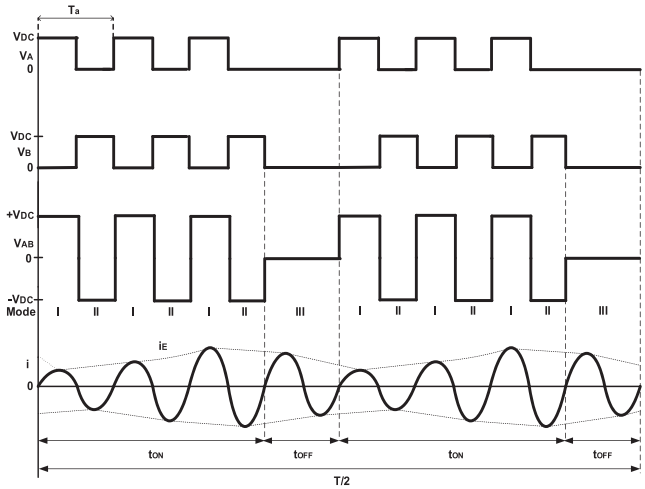

Fig. 5. Control principle of PDM technique.

In Mode I, S_1 and S_4 switches are ON, while in Mode II, S_2 and S_3 switches are ON. In Mode III, the inverter output voltage (V_{AB}) is zero. Mode III operating condition is the natural response of the series RLC circuit. In this mode, the current is in damping form without receiving to zero for high Q. The control principle of PDM technique is shown in Fig. 5.

As seen in the figure, the square-wave voltage (Mode I and Mode II operation) is applied to the inverter in the three resonant cycles. The control pulse is deleted in the fourth cycle and zero voltage (Mode III) is applied to the inverter. When the four resonant cycle is considered, the output voltage of the inverter is in periodic waveform. The average output power is 3/4 when compared to full-power operation. In other words, the output power of the inverter is controlled by adjusting the pulse density of the square wave voltage.

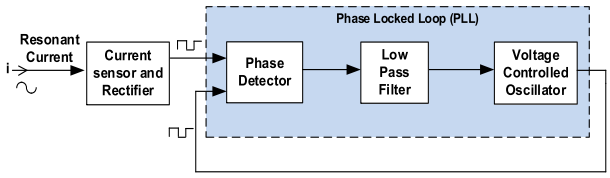

Fig. 6. Block diagram of the PLL control circuit.

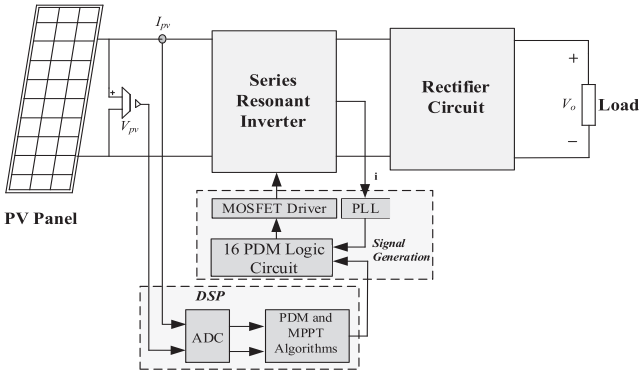

Fig. 7. Block diagram of the PDM-controlled MPPT system.

When the PDM control technique is applied to the series-resonant circuit with a quality factor much greater than 1 ($Q >> 1$), the resonant current is in sinusoidal form. In Fig. 5, resonant current is represented by (i) and the envelope of the resonant current is represented by i_E. Therefore, resonant current and the average power are obtained as follows [31]:

$$i(t) = i_E(t)\sin\omega_r t \tag{5}$$

$$P = \frac{1}{T}\int_0^T v_{AB}(t)i(t)dt. \tag{6}$$

C. PLL Control

PDM can efficiently be implemented by tracking the changing resonant conditions. For this purpose, PLL control should be used. The current signal on the resonant part is detected and the switching frequency is locked at the resonant frequency. Thus, the resonant frequency can be tracked. The block diagram of the PLL control circuit is given in Fig. 6.

PLL system used in PDM consists of three parts: phase detector, low-pass filter (LPF), and voltage-controlled oscillator (VCO). Phase difference between inverter voltage and current is detected and switching frequency is updated with VCO. If PLL is not used in PDM controller, the converter may operate below or above the resonant frequency. Therefore, ZCS conditions disappear [14], [31].

III. PDM-Controlled MPPT System

The block diagram of the PDM-controlled MPPT system is given in Fig. 7.

Both the 16 PDM patterns table and the PI-controlled P&O MPPT algorithm were written into the simplified C block in PSIM program. The flow diagram of the PI-controlled P&O MPPT algorithm adapted to the PDM technique and adjusted according to the small step reference voltage method is shown in Fig. 8.

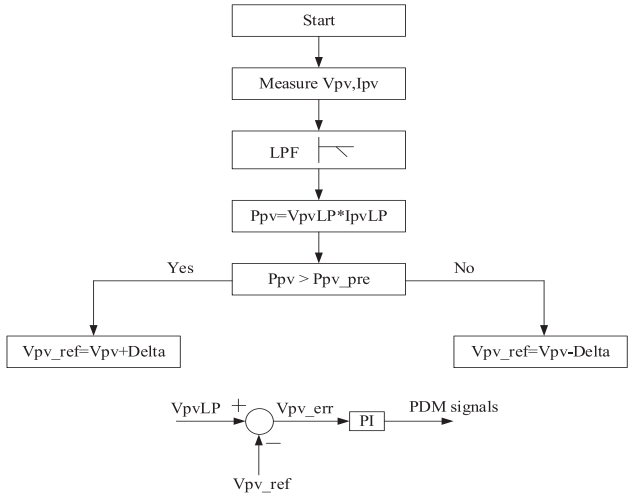

Fig. 8. Flow diagram of the PI-controlled P&O MPPT algorithm.

PI-controlled P&O MPPT algorithm is provided by adjusting the reference voltage according to power change. There may be interference in the current and voltage values measured from the PV panels. Low-pass filter was used in the system to ensure that MPP could be tracked accurately by eliminating these interferences. If both power and voltage increase, the pulse density ratio also increases. If both power and voltage decrease, the pulse density ratio increases. In other cases, pulse density ratio decreases. Thus, the maximum power to be obtained from the PV panel is provided by the PDM control technique and maximum power is transferred to the load.

The increase or decrease of pulse density was performed by adjusting the reference voltage depending on the power change. The difference between the filtered PV voltage and the value of the obtained reference voltage (V_{pv_ref}) gives the error value. The error voltage value is passed through the PI controller to generate PDM signals. If the power change is greater than zero, the determined delta value is added to the V_{pv} value to increase the pulse density. If the power change is less than zero, the pulse density is reduced by subtracting the delta value from V_{pv}.

IV. Analysis and Control of Single-Phase Grid-Tied Inverter System

Grid-tied inverters operate in parallel connected with the grid and have the ability to transfer the energy produced by the energy source to the grid. They operate efficiently since the surplus energy can be transferred to the grid [32], [33]. The block scheme of the single-phase grid-tied inverter circuit is presented in Fig. 9.

A. Determining the Parameters of LCL Filter

In grid-tied inverters, a filter must be used at the output of the inverter in order to transfer the current to the grid according to international standards such as IEC 61727, IEEE 1547-2003,

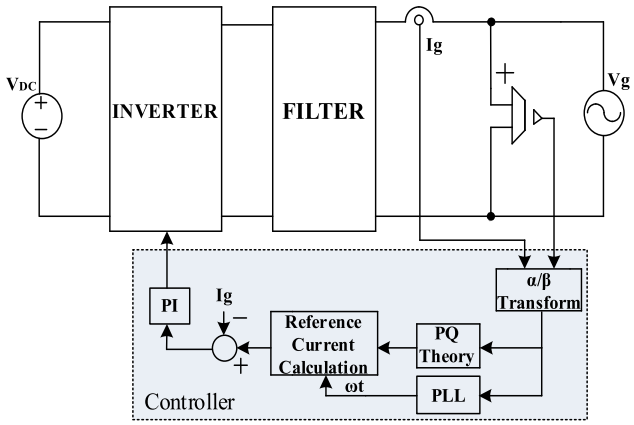

Fig. 9. Block scheme of the single-phase grid-tied inverter circuit.

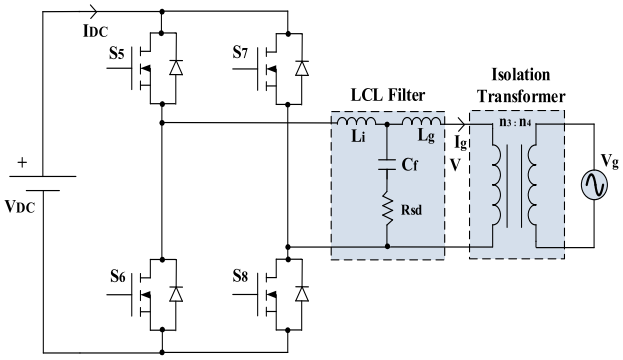

Fig. 10. Single-phase inverter with LCL filter.

TABLE I
PARAMETERS VALUES REQUIRED FOR INVERTER CIRCUIT

Parameters	Symbol	Values
Power	P_n	600 W
Inverter output voltage	V	110 V
DC Bus voltage	V_{DC}	400 V
Grid frequency	f	50 Hz
Switching frequency	f_{SW}	10 kHz

and IEEE 929-2000. Inverter output filters can be examined in four groups as L, LC, LCL, and LLCL [17].

Filters have advantages and disadvantages compared to each other. L filter's transfer function solution and design are easier than other filters. If the inductance value is small in L filter, the switching frequency of the inverter must be high. This increases the cost of the system and makes the design difficult. In order to eliminate these disadvantages, the filter inductance value must be increased. However, a larger inductance value of the filter ensures that the system becomes heavy and does not reduce its cost. Moreover, it is very difficult to achieve international standard values with L filter [34], [35].

The LC filter is a second-order filter and is generally preferred in power supply and OFF-grid systems. The LC filter used in grid-tied systems creates some problems. One of these problems is that when an inductor is connected parallel to the filter capacitor, high-frequency harmonics occur even if low impedance is achieved at high frequencies. This leads to high inrush currents. Another problem is that the inductance of the grid is connected to the LC filter in series. Therefore, even if the LC filter is connected to the system, the LCL filter condition occurs. As a result, it is difficult to analyze and design the grid-tied LC filter [35]–[37].

LCL filter is among the most commonly used filter type. This filter is a third-order filter and is smaller in size than other filter types. However, it is more complicated to determine the parameters of the LCL filter. Moreover, the parameters must be calculated correctly so that the system provides steady state [38]. With the LLCL filter, the cost and size are minimal and the harmonics are better filtered. However, it is very difficult for the system to provide steady state [39].

Considering the factors such as cost and size of the system and the steady-state condition, LCL filter is preferred for the design of a single-phase grid-tied inverter. The single-phase grid-tied inverter with LCL filter is shown in Fig. 10.

The parameters of the single-phase inverter must be determined before determining the LCL filter parameters. Design parameters are given in Table I.

To apply the LCL filter parameters calculated mathematically, the circuit was designed as $L_i = 3.25$ mH, $C_f = 8$ μF, and $L_g = 2.5$ mH. The ratio of the isolation transformer used in the system was 1:2. After the parameters of the LCL filter are determined, the resonant frequency can be calculated. Resonant frequency is calculated by the following formula:

$$f_{\text{res}} = \frac{1}{2\pi}\sqrt{\frac{L_i + L_g}{L_i.L_g.C_f}}. \tag{7}$$

The resonant frequency should be between the intervals shown in (8) [40], [41]

$$10f < f_{\text{res}} < 0.5f_{\text{sw}}. \tag{8}$$

A series resistor is connected to the capacitor in order to reduce the oscillations and to prevent the unstable state of the filter. This solution is called as "passive damping." Although it is a simple and reliable solution, it decreases the filter efficiency due to the increase of heating losses. Passive damping creates a considerable amount of power loss for high-power applications, while power loss for low-power applications can be neglected. Passive damping resistor (R_{sd}) is calculated as in (9) [41]–[43]

$$R_{\text{sd}} \geq \frac{1}{3.\omega_{\text{res}}.C_f}. \tag{9}$$

B. T/4 Delay PLL and Active Power Control

In order to be synchronized with the grid, PLL must be used in the grid-tied inverters. PLL algorithm provides the control of the grid frequency. Many PLL algorithms are used for inverters. T/4 delay PLL is one of the algorithms that can be used to obtain phase angle in single-phase applications. α–β and *d*–*q* axis frames are required in T/4 delay PLL algorithm [44], [45]. First, in order to form the PLL algorithm, the α–β axis frame must be obtained. In single-phase systems, the orthogonal signal of the time-based current or voltage cannot be obtained. Therefore, an

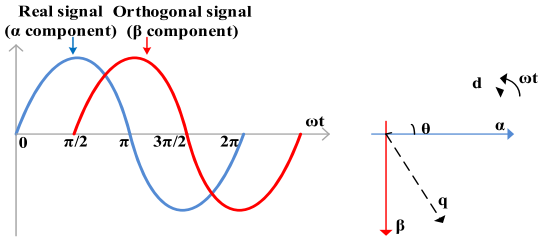

Fig. 11. Vectorial representation of *d–q* axis frames with real and orthogonal signals.

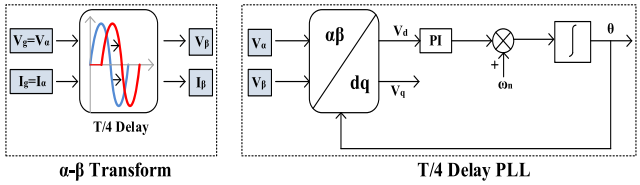

Fig. 12. α–β transform and the T/4 delay PLL structure.

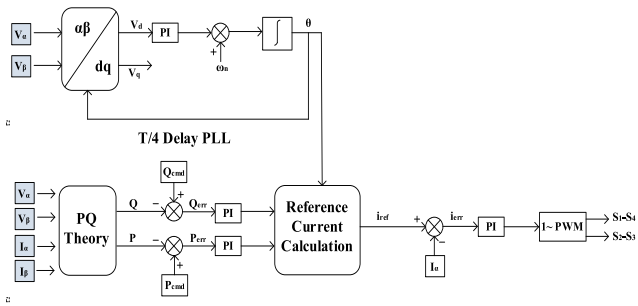

Fig. 13. Control block scheme of the single-phase grid-tied inverter.

imaginary orthogonal signal (β component) must be obtained. For this purpose, the α component must be shifted as $\pi/2$. In this case, two components are obtained. The α component is on the real, and the β component is on the imaginary axis. *d–q* axis frames with real and imaginary signals are given in Fig. 11 [46].

The orthogonal signal was obtained by using T/4 delay in the system. The grid voltage (V_g) is taken as V_α. V_β is obtained by the shift of $\pi/2$. In T/4 delay PLL circuit, (10) was utilized to transform the α–β to *d–q* axis frame by Park transform [47]. Fig. 12 shows the α–β transform and the T/4 delay PLL structure

$$\begin{bmatrix} V_d \\ V_q \end{bmatrix} = \begin{bmatrix} \cos\theta & \sin\theta \\ -\sin\theta & \cos\theta \end{bmatrix} \begin{bmatrix} V_\alpha \\ V_\beta \end{bmatrix}. \tag{10}$$

The control block scheme of the designed system is presented in Fig. 13.

Active-reactive power (*PQ* theory) calculation was provided using the V_α, V_β, I_α, and I_β values. The calculated power values are given in (11)

$$\begin{aligned} P &= \frac{1}{2}(V_\alpha I_\alpha + V_\beta I_\beta) \\ Q &= -\frac{1}{2}(V_\alpha I_\beta + V_\beta I_\alpha). \end{aligned} \tag{11}$$

The obtained power values were compared with the desired power values ($P_{\rm cmd}$ and $Q_{\rm cmd}$) and error values were obtained. The reference power value ($P_{\rm ref}$) used in the reference current calculation is equal to the desired power value $(P_{\rm cmd})$ $(P_{\rm ref} = P_{\rm cmd})$. In this article, $Q_{\rm cmd}$ was taken as zero since reactive power control was not performed. The power error was compensated with PI controller and included in the ωt formulas obtained from the PLL algorithm. Reference current formula was found using the following equations [48]:

$$\phi = \tan^{-1}\left(\frac{Q_{\rm ref}}{P_{\rm ref}}\right) \tag{12}$$

$$I_g = \frac{P_{\rm ref}}{V_q \cos\phi} \tag{13}$$

$$i_{\rm ref} = \sqrt{2} I_g \sin(\omega t - \phi). \tag{14}$$

Difference between I_α and $i_{\rm ref}$ gives the current error. The error current is compensated with PI current controller, and thus switching signals are generated.

V. Implementation of Grid-Tied Inverter With PDM-Controlled MPPT

Simulation and application studies of full-bridge series-resonant power converter operating at resonant frequency by PDM control technique at different solar radiation values with 600 W PV panel were performed. The switching frequency of PI current-controlled single-phase inverter was determined as 10 kHz and application studies were performed according to this frequency. Block diagram of single-phase grid-tied inverter system and MPPT- with PDM-controlled resonant converter are given in Fig. 14.

PDM signals were generated in the system according to the MPPT algorithm. A PDM logic circuit board was designed so that the switching signals of the circuit could be generated quickly according to the PDM signals. CD4046 was used for the PLL circuit.

Resonant inductor was determined as 115 μH while the resonant capacitor was determined as 16.46 nF. The ratio of high-frequency transformer was 1: 4. IRFP 260N MOSFETs were used for series-resonant converter circuit while IRFP 460N MOSFETs power switches were used for single-phase inverter circuit. 6N137 optocouplers and TC4429 drivers were used for both resonant converter and inverter circuits. IXYS DSEI60-12 A diodes were used in rectifier circuit for series-resonant converter circuit. The control of both resonant converter and single-phase inverter was conducted by TMS320F28335 DSP control board. ACS712 and LV25-P sensor were used to measure the current and voltage of PV panels. ACS756SCA and LV25-P Hall effect sensors were used to measure the single-phase current–voltage and dc bus voltage.

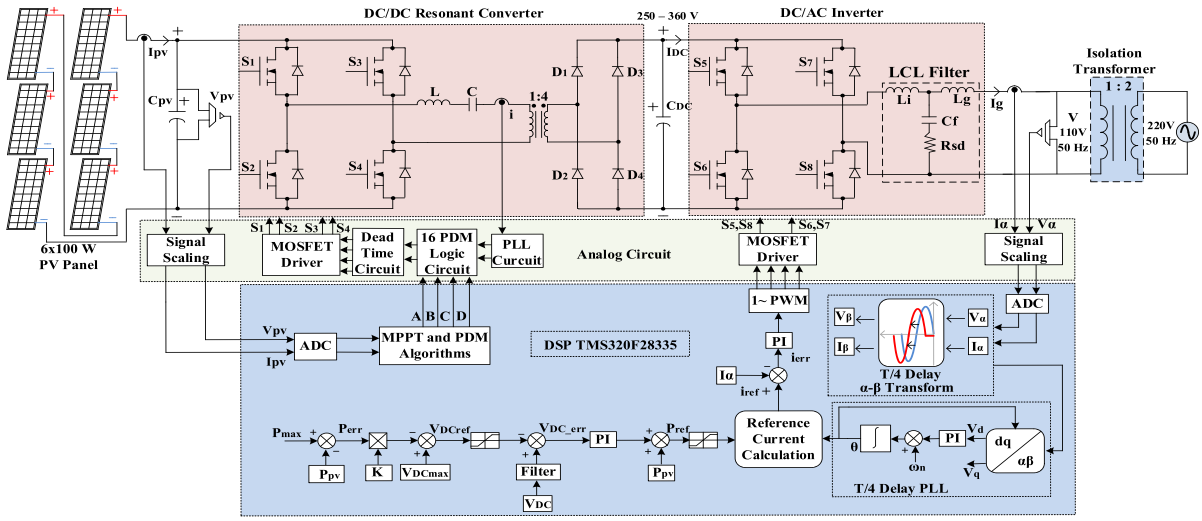

Fig. 14. Block diagram of the system.

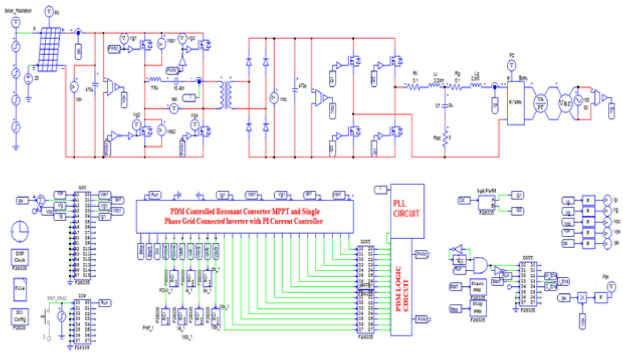

Fig. 15. Simulation screen image of the designed system.

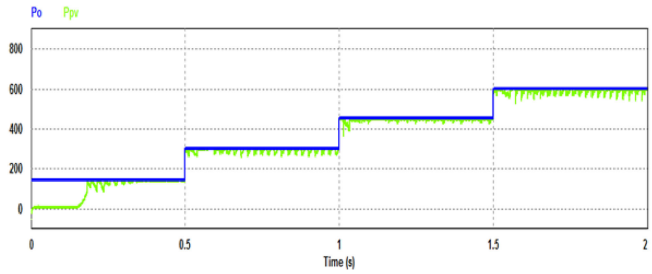

Fig. 16. Maximum power tracking.

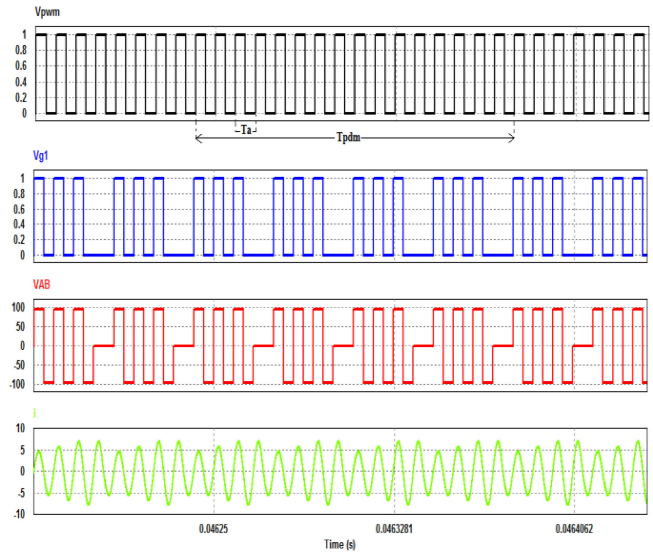

Fig. 17. 500 W/m^2, PWM, gate control signal, V_{AB} voltage, and resonant current.

VI. Simulation and Experimental Results

Simulation of the designed system was carried out using PSIM 10.0 program. The codes required for the control of the system were written in the simplified C block to generate embedded codes for DSP. Simulation screen image of the designed system is shown in Fig. 15.

In the simulation study, the solar radiation of the PV panels was adjusted as 250–500–750 and 1000 W/m^2 respectively. The simulation result with maximum power tracking depending on the gradual change of the solar radiation level is given in Fig. 16. In the simulation study, theoretical PV panel power is represented by (P_o) and PV panel power tracking the theoretical power is represented by (P_{pv}).

In order to obtain maximum power from PV panels in the solar radiation at 500 W/m^2, the pulse density ratio was set to be 12/16. As seen in Fig. 17, four control pulses were deleted according to the power required by the PV panel and the panels were operated at MPP. Simulation results of the PWM, gate control signal of the MOSFET, inverter output voltage (V_{AB}), and resonant current (i) for the measurement of 500 W/m^2 solar radiation level are shown in Fig. 17.

Fig. 18 shows the simulation image showing that switching is achieved at ZCS.

In order to obtain maximum power from the PV panels in the solar radiation at 750 W/m^2, the pulse density ratio was set to

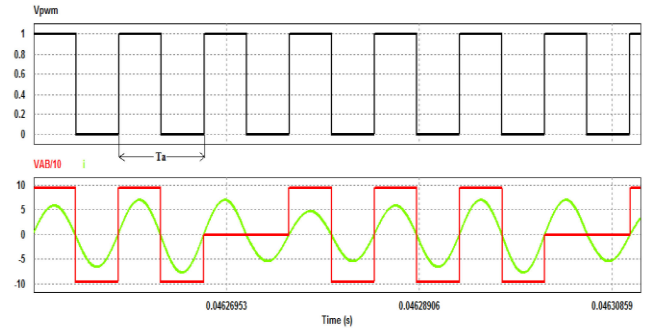

Fig. 18. PWM signal, V_{AB} voltage, and resonant current.

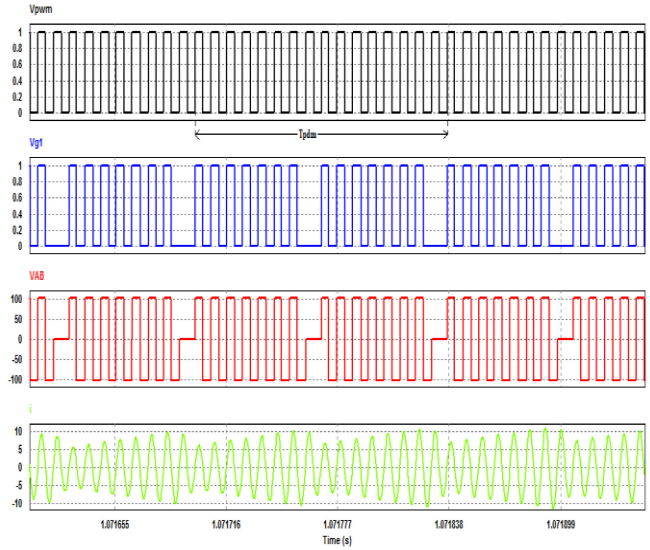

Fig. 19. 750 W/m^2, PWM, gate control signal, V_{AB} voltage, and resonant current.

be 14/16. As seen in Fig. 19, two control pulses were deleted according to the power required by the PV panel and the panels were operated at MPP. Simulation results for the measurement of 750 W/m^2 solar radiation are shown in Fig. 19.

Fig. 20 shows the results for 1000 W/m^2. As seen from the results, the converter is controlled with 16/16 PDM.

Fig. 21 shows the simulation image showing that switching is achieved at ZCS.

The maximum power obtained from PV panels depending on the solar radiation change was transferred to 110 V 50 Hz ac. The waveforms of the current and voltage transferred to the grid at the solar radiation values of 250–500–750 and 1000 W/m^2 are given in Fig. 22.

Fig. 23 shows the PV panel power (blue color), the power value tracked by the PDM-controlled P&O MPPT algorithm (green color), and the output power (red color) of the system.

In order to make simulation results similar to experimental values, catalog values of all the elements used in the system were used in the simulation and none of the values was accepted as ideal. According to the simulation result in Fig. 23, the MPPT efficiency for the condition at 500 W/m^2 solar radiation was found as 98.61% and the efficiency of the whole converter

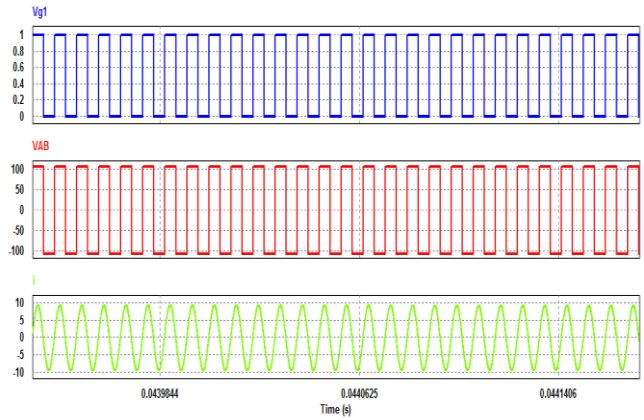

Fig. 20. 1000 W/m^2, gate control signal, V_{AB} voltage, and resonant current.

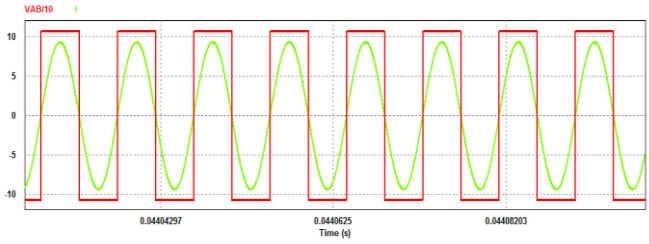

Fig. 21. 1000 W/m^2 radiation ZCS, V_{AB} voltage, and resonant current.

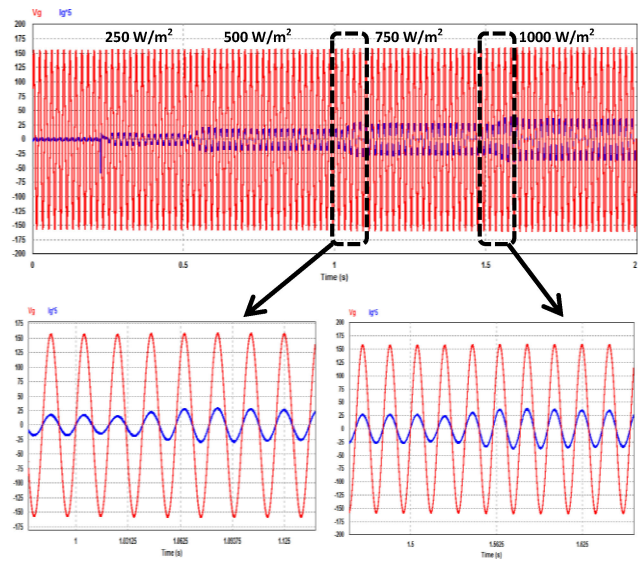

Fig. 22. Inverter output current and voltage for different power values.

was obtained as 93.55% while the system efficiency was found as 92.25%. On the other hand, the MPPT efficiency for the condition at 750 W/m^2 solar radiation was found as 99.53% and the efficiency of the whole converter was obtained as 93.44% while the system efficiency was found as 93%. Moreover, the MPPT efficiency at 1000 W/m^2 solar radiation was found as 99.8% and the efficiency of the whole converter was obtained as 92.32% while the system efficiency was found as 92.14%.

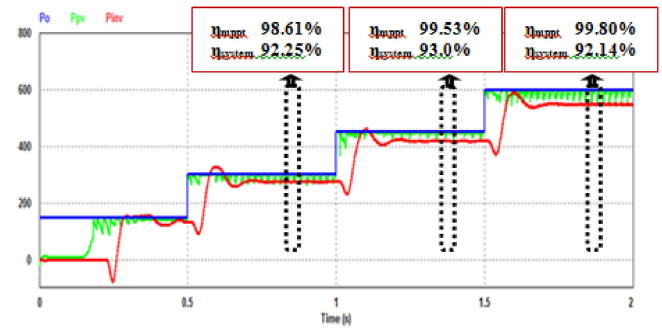

Fig. 23. PV panel power, power with MPPT algorithm, and the output power of the system.

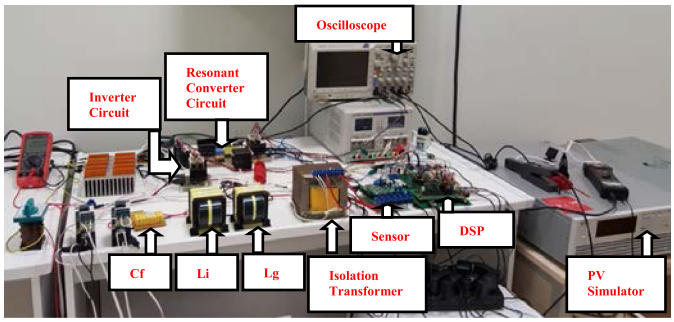

Fig. 24. Experimental setup of the system.

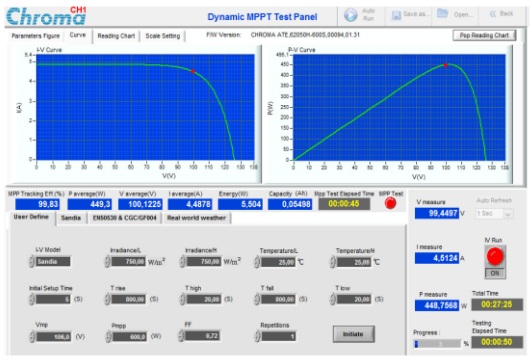

Fig. 25. Screen image obtained from simulator at 750 W/m^2 solar radiation.

The experimental setup of a single-phase grid-tied inverter circuit with resonant converter MPPT is shown in Fig. 24.

A 5 kW PV simulator of the Chroma 62050H-600S was used to determine the extent to which the MPPT process could be performed in the system. PV simulator interface enabled the information of whether the system was at MPP and the dynamic structure of MPPT algorithm. In addition, PV simulator provided the tracking of MPPT algorithm efficiency, panel current, voltage, and power. Screen image of the values obtained from the PV simulator at 750 W/m^2 solar radiation is given in Fig. 25.

As seen in the screen image, the MPPT efficiency was 99.83%. The oscilloscope images of the gate-source voltage, inverter output voltage (V_{AB}), resonant current, and dc bus voltage for this solar radiation level are presented in Fig. 26.

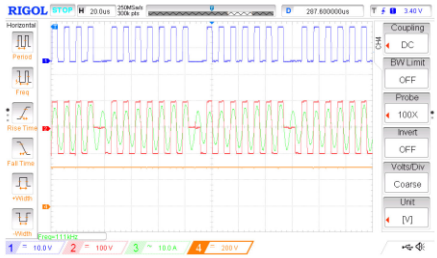

Fig. 26. 750 W/m^2, gate-source voltage (CH1), V_{AB} voltage (CH2), resonant current (CH3), and dc bus voltage (CH4).

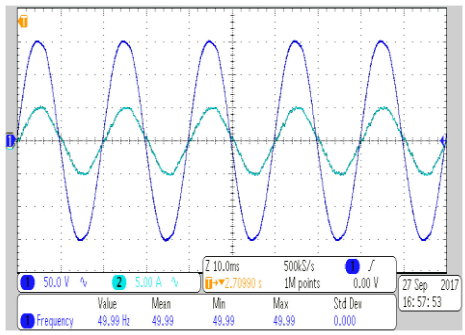

Fig. 27. Current and voltage transferred to the grid at 750 W/m^2 solar radiation.

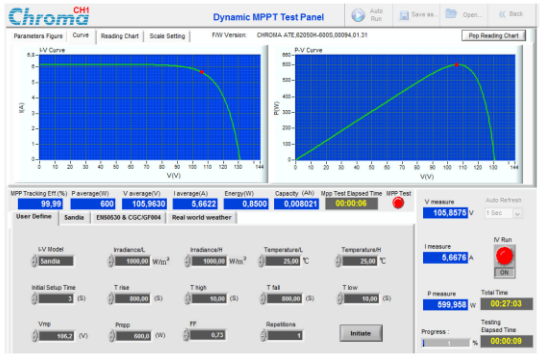

Fig. 28. Screen image of the values obtained from simulator at 1000 W/m^2 solar radiation level.

As can be seen from the measurements, the pulse density ratio was 14/16 to achieve maximum power at 750 W/m^2 solar radiation. Meanwhile, the switching frequency was at 111 kHz.

Oscilloscope image of the current and voltage measured from the grid when the power obtained from the PV panels was transferred to the grid is given in Fig. 27.

Screen images of the values obtained from PV simulator at 1000 W/m^2 solar radiation are presented in Fig. 28.

As seen in the screen image, the MPPT efficiency was 99.9%. Oscilloscope image of gate-source voltage, inverter output voltage (V_{AB}), and resonant current for this solar radiation level are given in Fig. 29.

In Fig. 29, the switching frequency is at 111 kHz. Oscilloscope image of the current and voltage measured from the grid when the power obtained from the PV panels was transferred to the grid is given in Fig. 30.

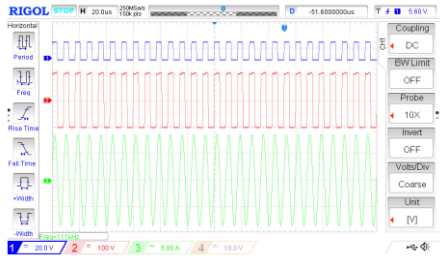

Fig. 29. 1000 W/m^2, gate-source voltage (CH1), V_{AB} voltage (CH2), and resonant current (CH3).

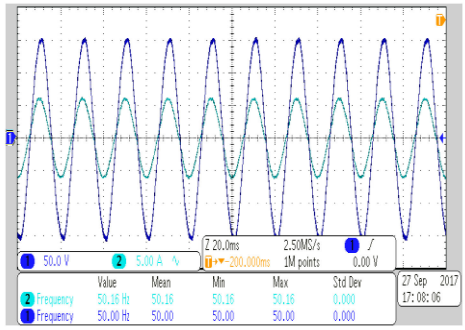

Fig. 30. Current and voltage transferred to the grid at 1000 W/m^2 solar radiation.

As seen from experimental and simulation studies, electrical energy obtained from PV panels was transferred to single-phase grid with high-frequency resonant converter MPPT system using the PDM control technique.

VII. Conclusion

In this article, energy obtained from PV panels operating continuously at MPP under different solar radiation conditions was transferred to a single-phase grid. MPPT with PDM-controlled resonant converter was designed and implemented to increase the limited operating frequency and overcome hard switching conditions, which are among the problems of the conventional PWM-switched MPPTs. According to the MPPT algorithm, power control was performed by deleting some control pulses of the converter operating at resonant frequency by PDM technique. Therefore, ZCS conditions were achieved and the 600 W laboratory prototype system was operated at frequencies above 100 kHz. As the MPPT algorithm, P&O method was preferred which has simple software, high reliability, and efficiency. The PV simulator used in the system was adjusted, and PDM-controlled MPPT and series-resonant converter were tested under different solar irradiation values at the laboratory. The tracking efficiency of the MPPT algorithm was observed as $\eta_{\mathrm{MPPT}} = 99\%$ and above. An LCL filter was used at the output of the inverter in order to transfer the maximum power obtained from PV panels to single-phase grid. The following results were obtained from the study in which the design of MPPT with resonant converter and single-phase grid-tied inverter was realized.

1) MPP tracking in the designed series-resonant converter was provided by operating at resonant frequency and ZCS was kept continuously.
2) The effect of PDM control algorithm on MPPT performance was examined in resonant converter. It was found that the tracking efficiency of P&O MPPT algorithm operating at different solar radiation conditions and constant frequency was high.
3) The prototype-resonant converter was operated above 100 kHz frequency by low switching stress as a result of soft switching condition.
4) PDM-controlled MPPT and single-phase inverter were cascaded and therefore the energy produced by PV panels was transferred to the single-phase grid.

References

[1] M. Papież, S. Śmiech, and K. Frodyma, "Determinants of renewable energy development in the EU countries. A 20-year perspective," *Renew. Sustain. Energy Rev.*, vol. 91, pp. 918–934, Aug. 2018.

[2] A. R. Nadia, N. A. M. Isa, and M. K. M. Desa, "Advances in solar photovoltaic tracking systems: A review," *Renew. Sustain. Energy Rev.*, vol. 82, pp. 2548–2569, Feb. 2018.

[3] H. Ozbay, A. Karafil, Y. Onal, M. Kesler, and H. Parmaksiz, "The monitoring of monthly, seasonal, and yearly optimum tilt angles by raspberry Pi card for Bilecik city, Turkey," *Energy Procedia*, vol. 113, pp. 311–318, May 2017.

[4] M. Das and V. Agarwal, "Novel high-performance stand-alone solar PV system with high-gain high-efficiency DC–DC converter power stages," *IEEE Trans. Ind. Appl.*, vol. 51, no. 6, pp. 4718–4728, Nov./Dec. 2015.

[5] Q. Li, S. Zhao, M. Wang, Z. Zou, B. Wang, and Q. Chen, "An improved perturbation and observation maximum power point tracking algorithm based on a PV module four-parameter model for higher efficiency," *Appl. Energy*, vol. 195, pp. 523–537, 2017.

[6] H. Armghan, I. Ahmad, A. Armghan, S. Khan, and M. Arsalan, "Backstepping based non-linear control for maximum power point tracking in photovoltaic system," *Sol. Energy*, vol. 159, pp. 134–141, 2018.

[7] A. Belkaid, I. Colak, and O. Isik, "Photovoltaic maximum power point tracking under fast varying of solar radiation," *Appl. Energy*, vol. 179, pp. 523–530, 2016.

[8] J. Ahmed and Z. Salam, "An improved perturb and observe (P&O) maximum power point tracking (MPPT) algorithm for higher efficiency," *Appl. Energy*, vol. 150, pp. 97–108, Jul. 2015.

[9] M. H. Rashid, *Power Electronics Handbook Devices, Circuits, and Applications*, 3rd ed. Oxford, U.K.: Elsevier; 2011.

[10] M. K. Kazimierczuk and D. Czarkowski, *Resonant Power Converters*. New York, NY, USA: John Wiley & Sons, 2012.

[11] G. Bal and N. Öztürk, "A novel control technique for soft-switching sinusoidal pulse width modulation inverter," *Electr. Power Compon. Syst.*, vol. 39, no. 1, pp. 31–45, Jan. 2011.

[12] J. M. Alonso, M. S. Perdigão, D. G. Vaquero, A. J. Calleja, and E. S. Saraiva, "Analysis, design, and experimentation on constant-frequency DC–DC resonant converters with magnetic control," *IEEE Trans. Power Electron.*, vol. 27, no. 3, pp. 1369–1382, Mar. 2012.

[13] H. Fujita and H. Akagi, "Pulse-density-modulated power control of a 4 kW, 450 kHz voltage-source inverter for induction melting applications," *IEEE Trans. Ind. Appl.*, vol. 32, no. 2, pp. 279–286, Mar./Apr. 1996.

[14] S. Oncu and A. Karafil, "Pulse density modulation controlled converter for PV systems," *Int. J. Hydrogen Energy*, vol. 42, pp. 17823–17830, 2017.

[15] V. Esteve *et al.*, "Improving the efficiency of IGBT series-resonant inverters using pulse density modulation," *IEEE Trans. Ind. Electron.*, vol. 58, no. 3, pp. 979–987, Mar. 2011.

[16] J. Jana, H. Saha, and K. D. Bhattacharya, "A review of inverter topologies for single-phase grid-connected photovoltaic systems," *Renew. Sustain. Energy Rev.*, vol. 72, pp. 1256–1270, 2017.

[17] M. Büyük, A. Tan, M. Tümay, and K. Ç. Bayındır, "Topologies, generalized designs, passive and active damping methods of switching ripple filters for voltage source inverter: A comprehensive review," *Renew. Sustain. Energy Rev.*, vol. 62, pp. 46–69, 2016.

[18] P. Channegowda and V. John, "Filter optimization for grid interactive voltage source inverters," *IEEE Trans. Ind. Electron.*, vol. 57, no. 12, pp. 4106–4114, Dec. 2010.

[19] H. Athari, M. Niroomand, and M. Ataei, "Review and classification of control systems in grid-tied inverters," *Renew. Sustain. Energy Rev.*, vol. 72, pp. 1167–1176, May 2017.

[20] H. Li, J. Fang, S. Chen, K. Wang, and Y. Tang, "Pulse density modulation for maximum efficiency point tracking of wireless power transfer systems," *IEEE Trans. Power Electron.*, vol. 33, no. 6, pp. 5492–5501, Jun. 2018.
[21] S. Borekci, "Dimming electronic ballasts without striations," *IEEE Trans. Ind. Electron.*, vol. 56, no. 7, pp. 2464–2468, Jul. 2009.
[22] L. Korošec, T. Konjedic, M. Truntič, M. Rodič, and M. Milanovič, "Field programmable gate array-based control method for a pulse density modulated microinverter operating in island mode," *IET Power Electron*., vol. 9, no. 14, pp. 2621–2630, Nov. 2016.
[23] M. Fan, L. Shi, Z. Yin, and Y. Li, "A novel pulse density modulation with semi-bridgeless active rectifier in inductive power transfer system for rail vehicle," *CES Trans. Elect. Mach. Syst.*, vol. 1, no. 3, pp. 397–404, Dec. 2017.
[24] S. Jiang, D. Cao, Y. Li, and F. Z. Peng, "Grid-connected boost-half-bridge photovoltaic microinverter system using repetitive current control and maximum power point tracking," *IEEE Trans. Power Electron.*, vol. 27, no. 11, pp. 4711–4722, Nov. 2012.
[25] S. Hu, X. Li, and A. K. Bhat, "Operation of a bidirectional series-resonant converter with minimized tank current and wide ZVS range," *IEEE Trans. Power Electron.*, vol. 34, no. 1, pp. 904–915, Jan. 2019.
[26] H. Wang, T. Saha, B. Riar, and R. Zane, "Design considerations for current-regulated series-resonant converters with a constant input current," *IEEE Trans. Power Electron.*, vol. 34, no. 1, pp. 141–150, Jan. 2019.
[27] T. G. Subhash Joshi and V. John, "Circuit-parameter-based audiosusceptibility model for series resonant converter," *IEEE Trans. Power Electron.*, vol. 34, no. 6, pp. 5927–5939, Jun. 2019.
[28] S. H. Ryu, D. H. Kim, M. J. Kim, J. S. Kim, and B. K. Lee, "Adjustable frequency-duty-cycle hybrid control strategy for full-bridge series resonant converters in electric vehicle chargers," *IEEE Trans. Ind. Electron.*, vol. 61, no. 10, pp. 5354–5362, Oct. 2014.
[29] X. Li and A. K. Bhat, "Analysis and design of high-frequency isolated dual-bridge series resonant DC/DC converter," *IEEE Trans. Power Electron.*, vol. 25, no. 4, pp. 850–862, Apr. 2010.
[30] H. Y. Leung, D. McCormick, D. M. Budgett, and A. P. Hu, "Pulse density modulated control patterns for inductively powered implantable devices based on energy injection control," *IET Power Electron*., vol. 6, no. 6, pp. 1051–1057, 2013.
[31] A. Karafil, H. Ozbay, and S. Oncu, "Power control of resonant converter MPPT by pulse density modulation," in *Proc. 10th IEEE Int. Conf. Elect. Electron. Eng.*, 2017, pp. 360–364.
[32] S. B. Kjaer, J. K. Pedersen, and F. Blaabjerg, "A review of single-phase grid-connected inverters for photovoltaic modules," *IEEE Trans. Ind. Appl.*, vol. 41, no. 5, pp. 1292–1306, Sep./Oct. 2005.
[33] S. Kouro, J. I. Leon, D. Vinnikov, and L. G. Franquelo, "Grid-connected photovoltaic systems: An overview of recent research and emerging PV converter technology," *IEEE Ind. Electron. Mag.*, vol. 9, pp. 47–61, Mar. 2015.
[34] T. Lahlou, M. Abdelrahem, S. Valdes, and H. G. Herzog, "Filter design for grid-connected multilevel CHB inverter for battery energy storage systems," in *Proc. IEEE Int. Symp. Power Electron. Elect. Drives Automat. Motion*, Jun. 2016, pp. 831–836.
[35] O. Husev, A. Chub, E. Romero-Cadaval, C. Roncero-Clemente, and D. Vinnikov, "Voltage distortion approach for output filter design for off-grid and grid-connected PWM inverters," *J. Power Electron.*, vol. 15, no. 1, pp. 278–287, Jan. 2015.
[36] T. C. Wang, Z. Ye, G. Sinha, and X. Yuan, "Output filter design for a grid-interconnected three-phase inverter," in *Proc. IEEE 34th Annu. Conf. Power Electron. Specialist*, 2003, pp. 779–784.
[37] H. Cha and T. K. Vu, "Comparative analysis of low-pass output filter for single-phase grid-connected photovoltaic inverter," in *Proc. 25th Annu. IEEE Appl. Power Electron. Conf. Expo.*, 2010, pp. 1659–1665.
[38] A. Reznik, M. G. Simões, A. Al-Durra, and S. M. Muyeen, "LCL filter design and performance analysis for grid-interconnected systems," *IEEE Trans. Ind. Appl.*, vol. 50, no. 2, pp. 1225–1232, Mar./Apr. 2014.
[39] W. Wu, Y. He, and F. Blaabjerg, "An LLCL power filter for single-phase grid-tied inverter," *IEEE Trans. Power Electron.*, vol. 27, no. 2, pp. 782–789, Feb. 2012.
[40] J. F. Ardashir, M. Sabahi, S. H. Hosseini, F. Blaabjerg, E. Babaei, and G. B. Gharehpetian, "A single-phase transformerless inverter with charge pump circuit concept for grid-tied PV applications," *IEEE Trans. Ind. Electron.*, vol. 64, no. 7, pp. 5403–5415, Jul. 2017.
[41] E. Kantar, S. N. Usluer, and A. M. Hava, "Design and performance analysis of a grid connected PWM-VSI system," in *Proc. 8th IEEE Int. Conf. Elect. Electron. Eng.*, 2013, pp. 157–161.
[42] M. H. Mahlooji, H. R. Mohammadi, and M. Rahimi, "A review on modeling and control of grid-connected photovoltaic inverters with LCL filter," *Renewable Sustain. Energy Rev.*, vol. 81, no. 1, pp. 563–578, Jan. 2018.
[43] J. Y. Lee, Y. P. Cho, H. S. Kim, and J. H. Jung, "Design methodology of passive damped LCL filter using current controller for grid-connected three-phase voltage-source inverters," *J. Power Electron.*, vol. 18, no. 4, pp. 1178–1189, Jul. 2018.
[44] M. Ciobotaru, R. Teodorescu, and F. Blaabjerg, "Control of single-stage single-phase PV inverter," *EPE J.*, vol. 16, no. 3, pp. 20–26, Sep. 2006.
[45] Y. Yang and F. Blaabjerg, "Synchronization in single-phase grid-connected photovoltaic systems under grid faults," in *Proc. 3rd IEEE Int. Symp. Power Electron. Distrib. Gener. Syst.*, 2012, pp. 476–482.
[46] C. Roncero-Clemente, O. Husev, E. Romero-Cadaval, J. Zakis, D. Vinnikov, and M. I. Milanés-Montero, "Simulation study of the grid-connected single-phase impedance-sourced NPC inverter with different control methods," in *Proc. IEEE Int. Conf. Ind. Technol.*, 2015, pp. 2949–2954.
[47] Y. Yang, F. Blaabjerg, and Z. Zou, "Benchmarking of grid fault modes in single-phase grid-connected photovoltaic systems," *IEEE Trans. Ind. Appl.*, vol. 49, no. 5, pp. 2167–2176, Sep./Oct. 2013.
[48] M. C. Kisacikoglu, M. Kesler, and L. M. Tolbert, "Single-phase on-board bidirectional PEV charger for V2G reactive power operation," *IEEE Trans. Smart Grid*, vol. 6, no. 2, pp. 767–775, Mar. 2015.

Akif Karafil was born in Bursa, Turkey, in 1983. He received the B.S. degree in electrical education from Marmara University, İstanbul, Turkey, in 2007, the M.S. degree in electrical and electronics engineering from Karadeniz Technical University, Trabzon, Turkey, in 2011, and the Ph.D. degree in electrical and electronics engineering from Karabuk University, Karabuk, Turkey, in 2018.

He is working with Bilecik Seyh Edebali University Vocational High School, Bilecik, Turkey, where he is currently a Dr. Lecturer. His research interests include pulse density modulation control, resonant converters, soft switching, MPPT, single-phase grid-connected inverters, and PV system applications.

Harun Ozbay was born in Bursa, Turkey, in 1984. He received the B.S. degree in electrical education from Gazi University, Ankara, Turkey, in 2008, the M.S. degree in electrical education from Gazi University, Ankara, Turkey, in 2011, and the Ph.D. degree in electrical and electronics engineering from Karabuk University, Karabuk, Turkey, in 2017.

He is working with the Electrical Engineering Department, Bandirma Onyedi Eylul University, Balikesir, Turkey, where he is currently an Assistant Professor. His research interests include power electronics, resonant converters, electric machines, MPPT, grid-connected inverters and PV system applications, electric vehicles, and battery charger.

Selim Oncu was born in Zonguldak, Turkey, in 1978. He received the B.S. degree in electrical education from Gazi University, Ankara, Turkey, in 2001, the M.S. in electrical and electronics engineering from Pamukkale University, Denizli, Turkey, in 2005, and the Ph.D. degree in electrical education from Gazi University, Ankara, Turkey, in 2011.

He is working with the Electrical and Electronics Engineering Department, Karabuk University, Karabuk, Turkey, where he is currently an Associate Professor. His research interests include power electronics, resonant converters, induction heating systems, electronic ballasts, MPPT, grid-connected inverters, PV system applications, electric vehicle, and battery charger.